3D VELOCITY FIELD MEASUREMENT IN LARGE-SCALE ROTOR FLOWS

Reddy, U.C.[*] and Komerath, N.M.[+]
School of Aerospace Engineering
Georgia Institute of Technology
Atlanta, GA 30332-0150

Abstract

Planar velocity measurements in two rotorcraft flows are presented. The first is that of an isolated rotor in axial flight in a large settling chamber, with measurement parameters and test conditions typical of a full-scale rotor wake. The clean periodicity of this flow allows capture of fundamental vortex dynamics, as well as phase-resolved velocity measurements using an inexpensive white-light-based measurement system. The second flowfield is that of a rotor wake interacting with a fixed wing in a wind tunnel, representing many features of tiltrotor flows. This experiment was used as a test bed to develop and refine a technique to capture all 3 components of phase-resolved velocity over the volume of the interaction region. The velocity field is presented in several chordwise and spanwise sections as a function of rotor azimuth.

Introduction

Whole-field, multi-dimensional velocimetry continues to pose formidable challenges in rotorcraft flows. Though high-resolution, spatio-temporal techniques have been developed for laboratory-scale tests, large-scale applications are relatively unexplored due to the practical difficulties encountered in scaling up these techniques, and operating them under the constraints of real-life rotorcraft facility operation. The measurements and visualization presented in this paper were performed with a system which was developed specifically to enable operation under such constraints. Thus, high-power lasers, expensive scientific-grade cameras, and other high-cost, temperamental instrumentation are avoided.

Two experiments are discussed. The first was performed in a government facility, piggy-backed on a project to measure rotor performance. The entire test was completed in less than 1 week, from unpacking instrumentation to repacking it. The second is a wind tunnel experiment where a large number of measurement planes are captured, in a complex, periodic flowfield: here the primary challenges are in setting up so many measurement planes, and analyzing hundreds of image-pairs to obtain the full volume-resolved, 3D velocity field.

Isolated rotor in axial flight

Substantial uncertainties remain in modeling the wake of a helicopter rotor. Most of these can be traced to uncertainties regarding the structure and dynamics of the wake vortices, which pose challenging requirements of spatial and temporal resolution. The seemingly-simple case of a rotor in hover poses some of the biggest uncertainties. These arise from the suspicion that there may be fundamental instabilities in the vortex behavior. These instabilities are blamed for non-periodic phenomena, which in turn lead to measurements which show premature "diffusion" or dissipation of vortices. The large degree of flow unsteadiness observed in rotor hover tests, however, are usually accompanied by facility recirculation in indoor tests, and by wind effects outdoors. Whether due to basic or mundane causes, unsteadiness leads to substantial uncertainty in the measurement of hover performance, one of the most critical parameters in the design of a rotorcraft.

An experiment was performed in the Fall of 1996 (Ref. [1]) to see if the facility recirculation effects could be eliminated by extrapolating performance data obtained at finite climb speeds, to the case of hover (zero climb rate). A 2-bladed UH-1H model rotor was mounted axially in the settling chamber of the 7’ X 10’ #1 wind tunnel at NASA Ames Research Center. The rotor diameter is 2.08 m (82") and the settling chamber dimensions are 9.14 m X 9.45 m (30’ X 31’).

---

[*] Currently with GE Power Systems, Schenectady, NY
[+] Professor, School of Aerospace Engineering

Figure 1: Rotor mounted in settling chamber of 7' X 10' wind tunnel

Figure 1 shows the rotor centered in the settling chamber at a point 2.45 m upstream of the start of the contraction section. A uniform axial flow is achieved by running the low-speed tunnel. The tunnel contraction ratio of 13.29 translates the maximum test section velocity of about 91.44 m/s to a maximum rate-of-climb approaching 6.1 m/s. In this paper, the climb rate is non-dimensionalized by the rotor tip speed. For a rotor RPM of 1800 the tip speed and tip Mach number are 196.32 m/s and 0.6.

The rotor mount and test instrumentation in the tunnel are given in Ref. [1]. The flowfield was visualized using theatrical smoke with a pulsed white light system. This flow visualization set-up in the settling chamber is shown schematically in Figure 2. A radial cross-section of the rotor inflow/wake region was illuminated by two light sheets aligned such that they coincided in the measurement area. The measurement area was 2 m X 1.5 m.

The flow was seeded using theatrical fog generators far upstream of the rotor. Closer to the rotor a remotely-controlled single point smoke source was traversed to visualize tip vortices. A pair of intensified CCD cameras with externally triggered shutters were synchronized to each of the pulsed lights. The shutter of one camera was delayed from the other by a known time using a delay generator. Flow images were recorded on two VCRs for a range of delay times. The SCV technique is outlined and several demonstrations given in Ref. [2]. Application to unsteady, three-dimensional flows is dealt with in Ref. [3] - Ref. [6].

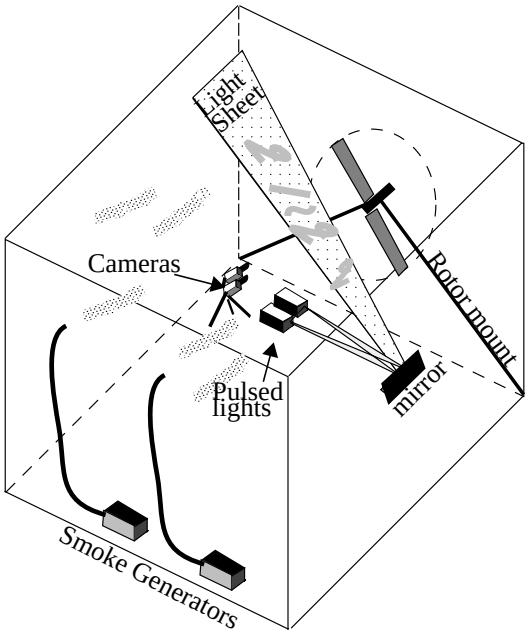

Figure 2: SCV set-up in the settling chamber

Flow Visualization

Flow visualization showed that the vortices from the two blades took different trajectories because of a mutual interaction process. The vortices from the two blades were seen to rotate about each other and merge into a single larger vortex. This vortex pairing was observed for a range of blade collectives as well as various freestream axial velocities. A sequence of images illustrating this process is shown in Figure 3.

These images were taken at a fixed collective of 11° and a non-dimensional climb rate of 0.0054. They are numbered in order of wake age with the odd and even numbered ones belonging to different blades. Figure 3 shows the initial phase where the two vortices roll up into a pair. In Figure 3(i) vortex 2 is beginning to catch up with 1. Vortex 4 has just been shed from the blade. In Figure 3(ii) 2 has begun to roll up with 1 and is already further downstream than 1. Vortices 3 and 4 are also convecting downstream. The counter rotating structure seen attached to vortex 3 is the outer edge of the inboard vortex sheet. This region rolls up as a counter rotating vortex of opposite sense and considerably weaker than the tip vortex. The counter rotating vortex is more pronounced in Figure 3(iii). In this image vortex 2 has completed a full rotation about vortex 1 since their positions relative to the blade are interchanged. Also seen is the birth of vortex 5.

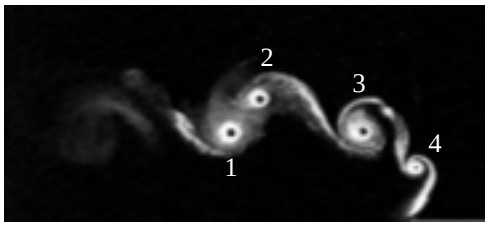

(i) Vortex 2 is starting to catchup with 1

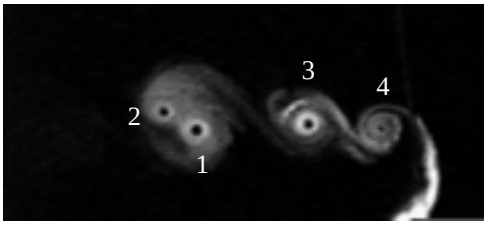

(ii) Vortex 2 over takes 1

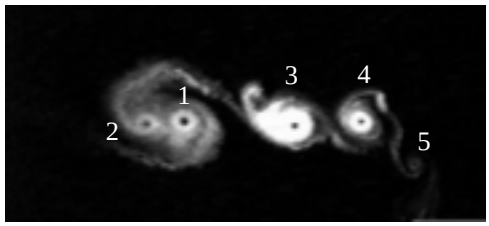

(iii) Vortex 2 completes a full rotation around 1

Figure 3: Vortex pairing sequence showing roll up

Effect of increasing collective

As the blade collective is increased gradually the location of vortex pairing shifts downstream. The flow visualization at a climb rate of 0.0054 in a radial plane at 74° to the horizontal is shown in Figure 4. The collective pitch of the rotor blade in degrees is displayed in the bottom right hand corner of the image. Four blade collective settings are shown - 4°, 6°, 8.2° and 9.9° in that order. Since the effective rate of climb is a function of rotor collective, it is not fixed throughout the collective sweep. In order to maintain a fixed climb rate throughout the collective sweep it is necessary to decouple the tunnel speed from the rotor power. This was achieved by installing a large flat plate to act as a throttle in the tunnel test section. The flow became visibly less steady when the throttle was installed.

The flow image at 4° collective shows the merged vortices for 3 previous rotor cycles. The wake expands with increasing collective and the pairing occurs at greater distances from the tip path plane. For a collective angle of 9.9° there are only two such merged vortices visible downstream of the vortex pair. All four images were obtained by using the rotor pulse to trigger the white lights. Different azimuth locations can be visualized by adjusting the phase difference between the lights and rotor pulse. In this case the rotor azimuth is the same as the light sheet orientation (74°) since the blade reflection is clearly visible in the light sheet.

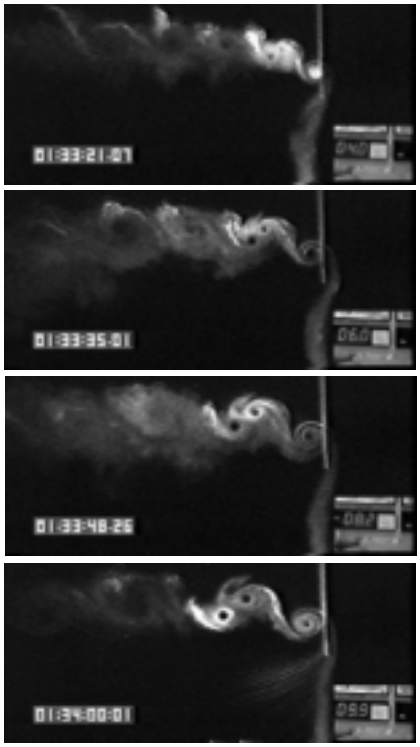

Figure 4: Effect of increasing blade collective

Effect of increasing climb rate

With higher freestream velocities the spacing between subsequent tip vortices is increased and consequently the onset of vortex pairing is considerably delayed. Figure 5 shows the wake structure at two climb rates for a blade collective of 11°. The first is at a climb rate of 0.3529 and the second at 0.5009. For the lowest climb rate case (0.0054) shown in Figure 3 & Figure 4, vortex pairing started beyond a wake age of 360°. At a climb rate of 0.3529 the pairing process begins beyond a wake age of 540° since there are three discrete tip vortices visible prior to pairing in Figure 5(a). For an even higher climb rate of 0.5009 the pairing is delayed further since there are atleast 5 unpaired vortices clearly visible in the wake (see Figure 5(b)). This indicates that pairing starts beyond 900° of

wake age in this case. In both cases vortex merger occurs outside the image area.

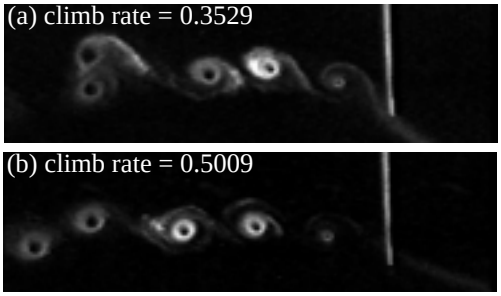

Figure 5: Effect of increasing climb rate

SCV Results

SCV measurements were made in a radial plane at 42.5° to the horizontal. The time delay between the two cameras was varied between 0 - 6 ms depending on the image magnification setting. Additional smoke from the fog generators located near the far wall of the settling chamber was used to capture the inflow and wake velocities. Sections of the video with sufficient seeding over most of the image area are chosen for SCV analysis. However at any given instant there are regions with little or no seeding. This is evident from the sample flow visualization image shown in Figure 6. The vortex sheet and tip vortices are clearly captured. The discrete turns of the helical wake are seen in the discontinuous smoke patterns.

The faint reflection of the rotor blade behind the light sheet is also seen in Figure 6. The bright region on the top of the image is due to light reflecting off the rotor hub. The video frame code used to match corresponding images for correlation is also seen in the top right hand corner. At the bottom right hand corner a picture of the rotor taken with the azimuth camera is mixed into the flow visualization image. This sample data is taken from a test at a climb rate of 0.015 and a blade collective of 11°. The SCV measurement area in this case is 2.03 m x 1.42 m with a 0.315 pixels/mm image magnification. The time delay between the two images correlated is 5 ms which corresponds to a rotor azimuth change of 54°. Thus the vector field shown is an average over this interval and is associated with the central azimuth of this range. The corresponding instantaneous velocity field is shown in Figure 7. The blank regions correspond to low seeding areas. The darker portions of this inverted-gray-sale image indicate areas of denser seeding. The outline of the rotor blade as seen in the flow visualization image is drawn.

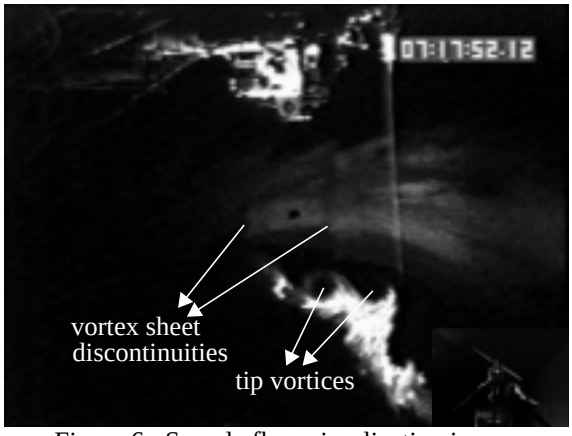

Figure 6: Sample flow visualization image

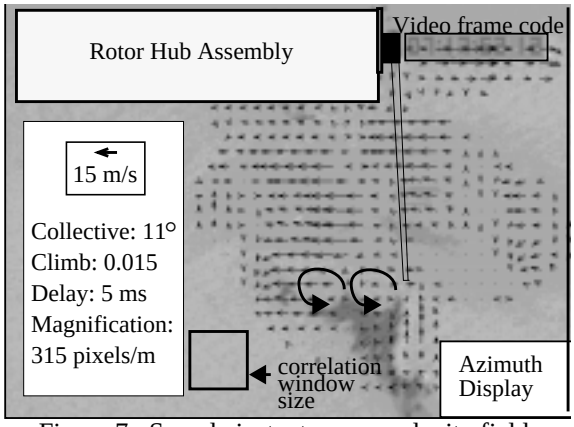

Figure 7: Sample instantaneous velocity field

Wake velocities on the order of 15 m/s were measured in regions of adequate flow seeding. Inflow velocities measured are in the 10 - 12 m/s range. Near the blade tip the two circular regions marked indicate locations of two tip vortices. Although some turning of the vectors is seen in this region, rotation in the tip vortices themselves is not captured. However, the translational velocity is captured since the vortex size is smaller than the size of the correlation window.

The rotor azimuth associated with each video frame was calculated by locating the blade-reflection frame. The blade-reflection frame is that in which the entire leading edge of the rotor blade is clearly reflected in the light sheet. The blade is parallel to the light sheet at azimuth. Azimuths for all consecutive frames are then calculated using the video framing rate (1/30 Hz) and rotor RPM. In this method however the two rotor blades cannot be distinguished from eachother and

therefore only azimuths between 0° and 180° can be obtained.

Phase resolved velocity fields at a climb rate of 0.015 and a blade collective of 11° are shown in Figure 8, 12, 13 and 14. These are taken at 0°, 45°, 90° and 135° azimuth bins. The 0° azimuth is when both rotor blades are horizontal. The maximum extent of the rotor blade is indicated in the figures (not actual position). The temporal resolution of this data is 43.2° and corresponds to a delay time of 4 ms. Each of these velocity fields is obtained by averaging 150 instantaneous velocity fields within a 45° azimuth bin. The origin is located at the rotor hub and all distances non-dimensionalized by rotor radius.

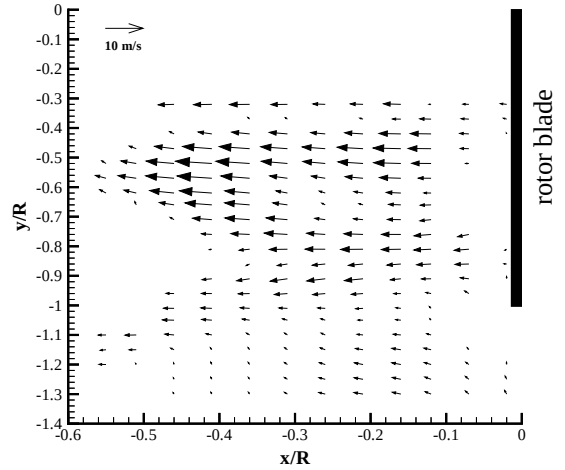

Figure 8: Ensemble averaged velocity field in a 45° bin centered at 0° azimuth

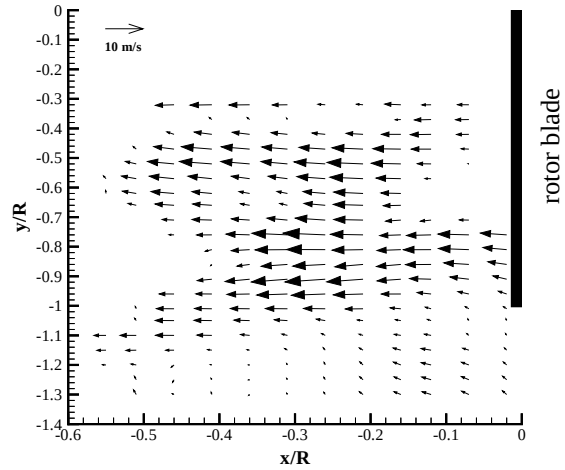

Figure 9: Ensemble averaged velocity field in a 45° bin centered at 45° azimuth

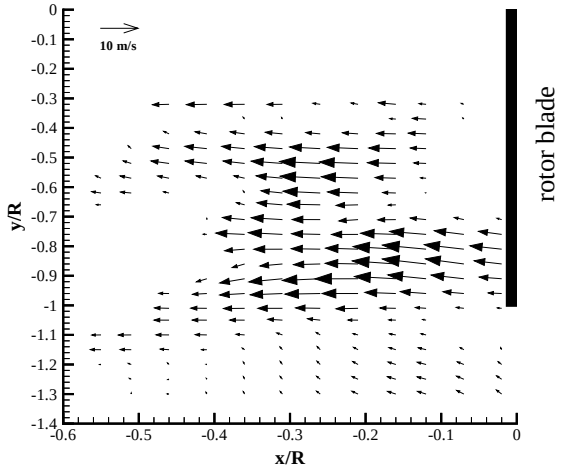

Figure 10: Ensemble averaged velocity field in a 45° bin centered at 90° azimuth

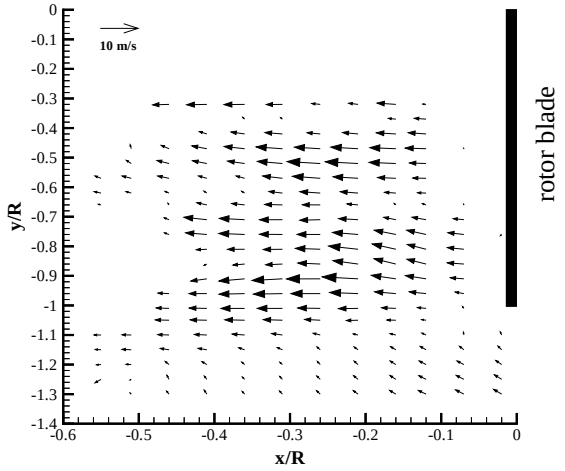

Figure 11: Ensemble averaged velocity field in a 45° bin centered at 135° azimuth

Vectors have been deleted in regions with low seeding (intensity < 15) and low correlation (correlation coefficient < 0.25). The variation in wake velocities with rotor azimuth is clearly seen. Wake velocities measured are in the 10 m/s range. The deflection of wake velocities near the blade tip as well as the decrease in velocity magnitude in this region is seen at all azimuths and indicates the presence of tip vortices. However the spatial resolution of the images is not sufficient to capture the rotation within the tip vortices.

Time averaged velocity field

Time averaged velocity fields were obtained by ensemble averaging 600 instantaneous vector fields. A time averaged velocity field for a blade collective of 11° blade and a climb rate of 0.0054 is shown in Figure 12. The time delay of 4 ms between images corresponds to an azimuth bin width of 43.2 .The parts of the image used to record rotor azimuth and video frame code are indicated. Spurious vectors in these regions are deleted. Vectors at the top of the image in the region of the hub assembly are also deleted. The location of the rotor blade, when it is seen in the light sheet, is drawn.

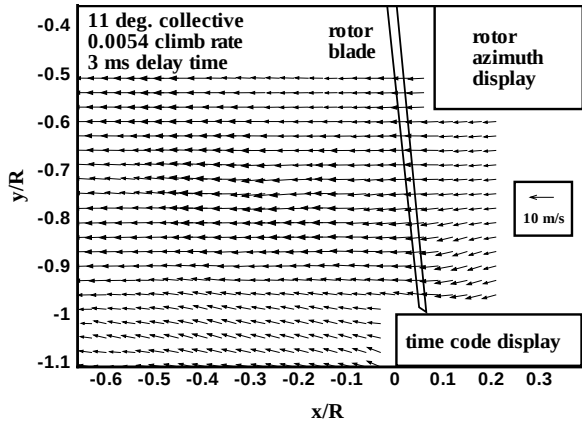

Figure 12: Time averaged velocity field at 11° collective and 0.0054 climb rate

The time averaged wake velocities reach 12 m/s. Wake contraction is seen in the deflection of the velocity vectors in the blade tip region. Inflow velocities are in the range of 8 m/s whereas wake velocities reach 12 m/s inboard of the blade tip and fall off on either side. The inflow profile at x/R = 0.03 is shown in Figure 13. The value from momentum theory is represented by the dashed line at 9.94 m/s.

Two profiles at different locations in the wake are shown in Figure 14. The profile just downstream of the blade (x/R = -0.03) shows maximum velocities at 85% of the blade radius. The velocity reaches a minimum near the blade tip and then increases gradually. This profile indicates the influence of a tip vortex inboard of the blade tip as seen in the flow visualization images. The peak velocities in the vortex are not captured due to limited spatial resolution of the velocity measurements but the vortex profile is captured. The profile further downstream (x/R = -0.33) has maximum velocities at about 78% of blade radius and does not show the vortex signature. The change in the radial location of maximum velocity between the two profiles is an indication of time-averaged wake contraction.

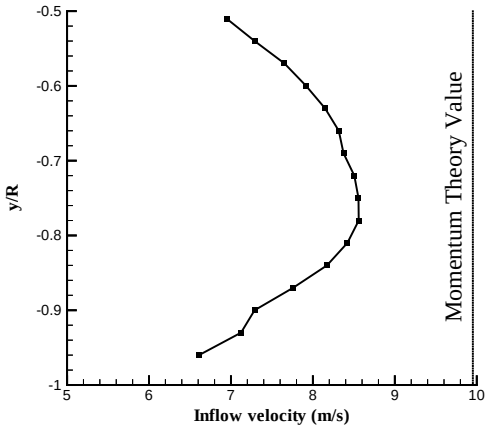

Figure 13: Inflow velocity profile at x/R = 0.03

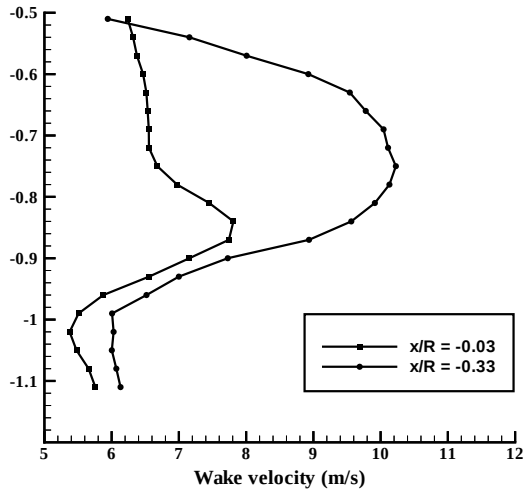

Figure 14: Wake velocity profile at two axial stations

The steadiness of the wake at low climb rates suggests that wake unsteadiness observed in rotor hover tests may be due to inflow contamination rather than being an intrinsic instability of the wake. As climb rate drops below 0.0014 the flow ceases to be steady. The figure-of-merit falls precipitously and the force balance gages show a sharp increase in both 2/rev and 6/rev loads. With decreasing climb rates the unsteadiness increases. The erratic changes in smoke patterns make tip vortex visualization difficult. In view of the degree of uncertainty in the data at hover, extrapolating low-climb rate data to hover is a more reliable method.

This test proved that full-scale rotorcraft flows are cleanly periodic when facility effects are eliminated. This finding adds significance to the method described in the next section to measure the 3-D velocity field in large-volume, periodic flows.

Third component method

There are different avenues to extend the planar SCV technique to 3D. Volumetric measurements via scanning of multiple planes is chosen as a tractable alternative for periodic flows. The repetition of events makes phase resolved measurements possible in spite of the finite time taken to step through different planes. Since the rotor and rotor/body flows investigated in this work have this periodicity, measurement of multiple planes of two component velocity fields using SCV is used as a precursor to the complete 3D three component velocity field measurement by solving the continuity equation. The procedure is described below.

A pulsed vertical light sheet is stepped normal to itself, and several images captured at each location. A second order finite difference scheme is used to compute the differential change in the (third) cross-plane component from one plane to the next. One sided difference was used at the edge points and central difference for the interior points. Boundary planes (where all three velocity components are measured or known) required for the numerical integration are obtained either by stepping the light sheet horizontally in the farfield or stepping it out vertically to a wall which forces the component perpendicular to the wall to be zero at the wall. The third component is specified at two boundary planes and then the continuity equation is integrated to yield the third component at all successive planes. Details of the technique including numerical validation and robustness to experimental noise are dealt with in Ref. [7].

Rotor-wing experiment

The experimental setup in the 2.1 m x 2.7 m (7' X 9') test section consists of a 2.23 m span NACA 0021 wing with 0.4 m chord at 0° angle of attack to the freestream direction, mounted below a two-bladed teetering rotor. The rotor hub is located 0.127 m upstream of the wing leading edge and centered at mid-span. The wing extends from wall to wall. Figure 15 shows the set-up in the test section. The rotor is driven by a 3 HP DC motor mounted on top of the tunnel. A feedback control system fixes the rotor speed within 1 RPM between 1000 and 2200 RPM. The rotor shaft is tilted at 6° to simulate forward flight. The 0.914 m diameter rotor has a constant chord of 0.0857 m and a NACA 0015 airfoil section. The blades are untwisted with a fixed collective of 10°. Rotor shaft vibration is monitored using two accelerometers. An optical trigger attached to the rotor system produces a once-per-revolution TTL pulse each time the rotor crosses the zero azimuth position.

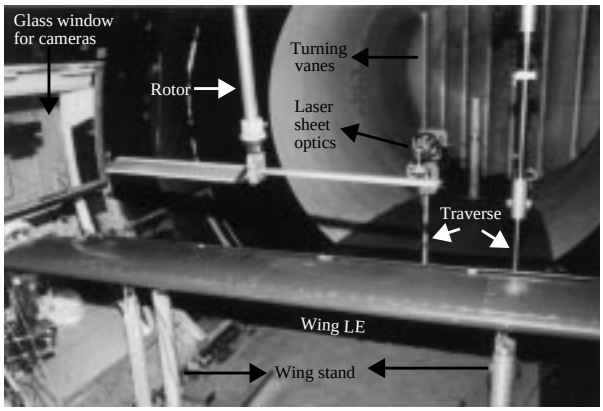

Figure 15: Rotor-wing setup in test section (view from upstream)

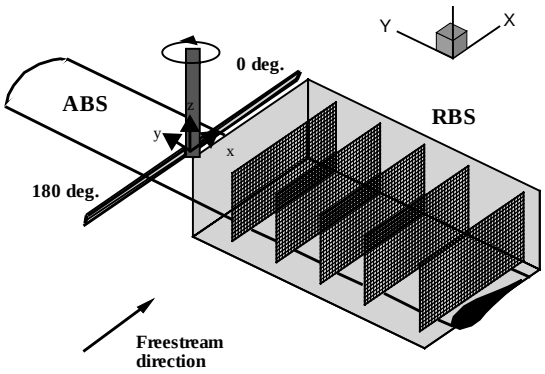

Figure 16: Orientation of chordwise data planes

The rotor wake region between the tip path plane and the wing surface was measured in several parallel chordwise vertical planes. The wing was at 0° angle of attack and the flap was not deflected. The wing of a tiltrotor corresponds to the RBS of the present configuration. The orientation of the data planes is shown in Figure 16. SCV data were taken at 15 azimuth intervals throughout the rotor cycle (24 azimuth bins in all) at all chordwise planes.

Seventeen data planes covering a wing span of 1.016 m on the RBS have been analyzed for a delay setting of 3.34 ms. The corresponding azimuth

resolution is 21.04°. A sample flow visualization image is shown in Figure 17. The wing surface and rotor hub are clearly visible in the light sheet and the blade position is drawn in. Any vectors obtained in the top portion of the image indicate the motion of the blade, azimuth disk and frame code display between the two images.

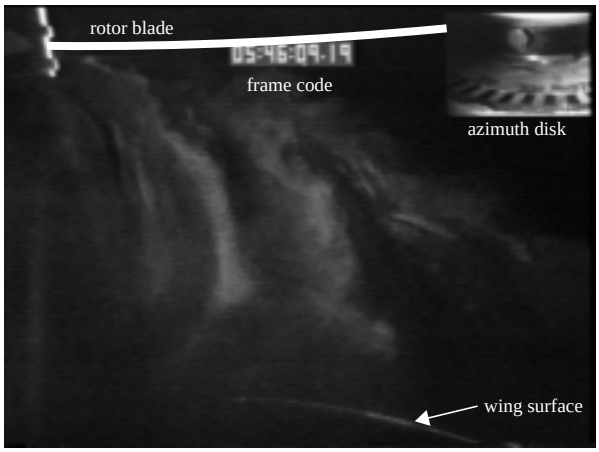

Figure 17: Chordwise flow visualization image at midspan (y/R=0)

SCV results

Instantaneous velocity data are sorted into 24 azimuth bins with a bin width of 21.04°. The bin width is essentially the angle covered by the rotor during the delay time between the two sets of images. A total of 600 image pairs are analyzed for each run and 25 velocity fields averaged in each azimuth bin. The azimuth angle associated with each ensemble averaged velocity field is the central azimuth of the bin.

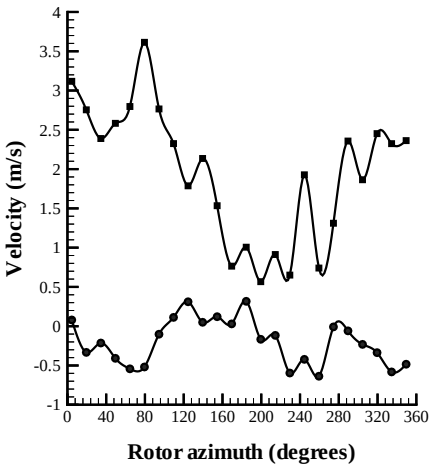

Figure 18: Streamwise and vertical velocity at x/R=0.22, y/R=0, z/R=0.28

Figure 18 shows the azimuthal variation of the ensemble averaged streamwise and vertical velocity components at a point x/R=0.22 and z/R=0.28 in the midspan plane. The once-per-rev variation is expected [8]: due to vortex interactions the flow pattern at a given point repeats only once per revolution. The variation is quite consistent, even though the individual values are picked off different vector fields.

This once-per-revolution variation is attributed to the separation of vortex trajectories from the two blades [9]. This phenomenon was clearly seen in the flow visualization. A pair of images taken 16.67 ms apart at the y/R=-0.61 plane are shown to illustrate this. The vortices are numbered in the order in which they are shed (1 and 3 are shed from one blade and 2 from the other). In Figure 19(a), vortex 1 is approaching the wing surface and vortex 2 and 3 are further away. In the second frame, 16.67 ms later, vortex 2 is progressing towards the leading edge of the wing whereas vortex 3 is following the trajectory of 1. The two trajectories are shown with dotted lines.

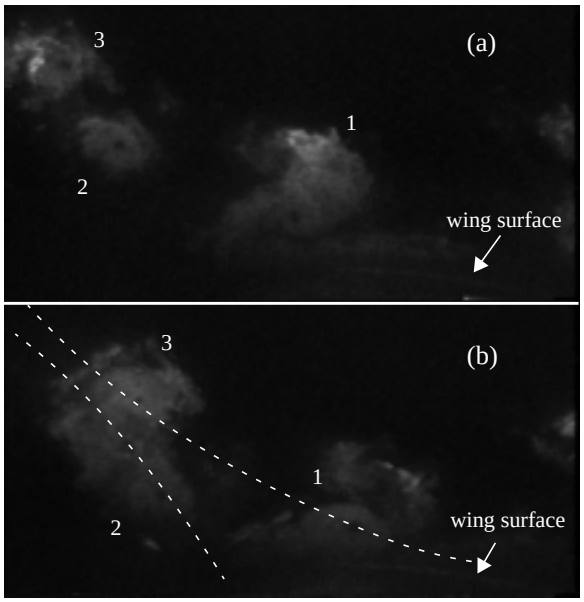

Figure 19: Separation of vortex trajectories

Chordwise-vertical velocity fields

Figure 20 - Figure 23 show 2D ensemble-averaged velocity fields overlaid on vorticity contours for two spanwise locations. Vorticity magnitude is computed from the two-component velocity data and is therefore limited by the resolution and accuracy limits of this data. Positive vorticity indicates a clockwise rotation and is represented by the dark portions of the contour plots. This is the direction of rotation of the tip

vortex shed from the rotor blade in the upstream position. Regions of negative vorticity seen throughout the flowfield indicate the presence of vortex sheets and the rolled-up vortices at their edges.

The temporal variation in the rotor wake at the y/R=-0.11 plane is seen by comparing Figure 20 and Figure 21. The regions of high positive vorticity over the wing indicate possible positions of the rotor tip vortex. There are two regions of high vorticity - one near the wing leading (seen clearly in Figure 21) and one further downstream. Their relative strengths vary with the rotor azimuth. These regions are seen at different stages of interaction with the wing at the different azimuths. In Figure 23 at the y/R=-0.56 plane the leading edge vortex is seen close to the wing surface. In Figure 22 however, this vortex appears to have just disappeared below the leading edge and the local upflow due to its clockwise rotation is seen. This indicates two vortex trails impinging on the wing - one that goes over the leading edge and the other convecting downstream over the wing surface.

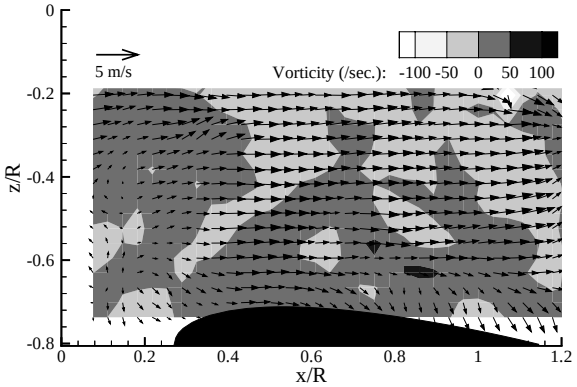

Figure 20: U and W components in the y/R=-0.11 plane at azimuth 10.82°

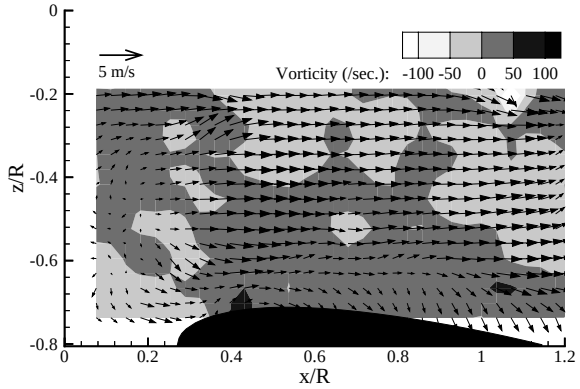

Figure 21: U and W components in the y/R=-0.11 plane at azimuth 325.82°

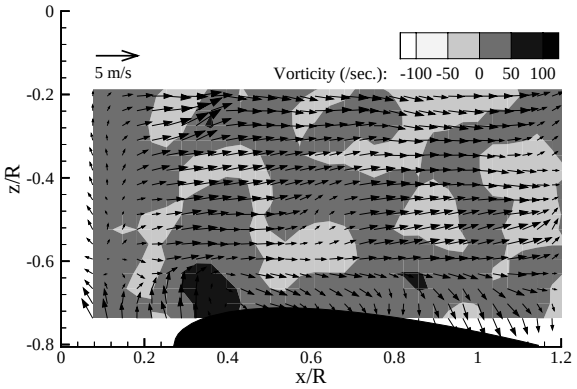

Figure 22: U and W components in the y/R=-0.56 plane at azimuth 9.48°

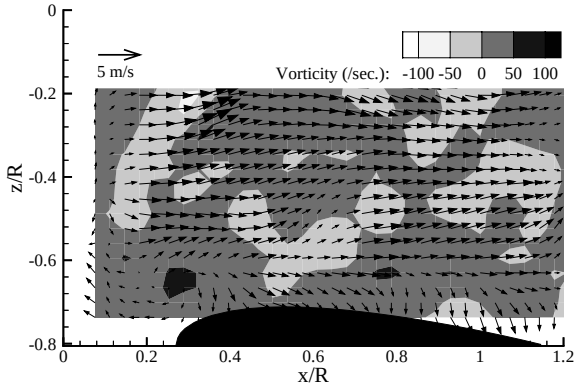

Figure 23: U and W components in the y/R=-0.56 plane at azimuth 324.48°

Spanwise component reconstruction

The spanwise velocity component on the RBS was reconstructed using the TVC method described in Chapter VI. The 17 SCV data planes on the RBS were input into the TVC solver using the two planes closest to the tunnel walls as boundary conditions. Boundary data were taken as close as possible to the tunnel walls. The last chordwise measurement plane was taken at y/R=-0.22. This is 7.62 cm inboard of the wing tip on the RBS. Due to lower gradients outside the rotor wake region the spacing between chordwise data planes was increased from 2.54 cm to 5.08 cm in this region. Polynomial interpolation was used between these planes to maintain a constant inter-plane spacing of 2.54 cm throughout the measurement volume. This increased the number of data planes from 17 to 21. The interpolated plane next to the boundary plane is taken as the second boundary plane required for the second

order finite difference scheme. A 3D measurement grid of 36 X 21 X 26 points is obtained at 24 points in the rotor cycle. The phase resolved spanwise-vertical velocity field at a few chordwise locations is presented in this section.

Two spanwise sections near the wing quarter chord (x/R=0.47) and mid-chord(x/R=0.72) are shown in Figure 24 and Figure 25. Two points of the rotor cycle at 9° and 324° are shown for each location. Figure 24 shows the spanwise velocities at 9° rotor azimuth. The flowfield shows the development of an outward flowing spanwise wall-jet profile. Near the quarter chord location the spanwise flow towards the RBS (left to right in figure) is confined to a small region above the wing surface. Further downstream both the velocity magnitudes as well as the physical extent of this flow have increased.

This trend continues up to the mid-chord location beyond which the spanwise flow towards RBS decreases and reduces to near zero at the trailing edge. As the wing trailing edge is approached the rotation of the wake induces spanwise flows directed towards ABS. The two streams of spanwise flow at different heights above the wing surface, one flowing towards the ABS and the other towards the RBS, are clearly seen at a rotor azimuth of 324° shown in Figure 25. Similar trends are seen at the other azimuths although there is substantial fluctuation in velocity magnitude.

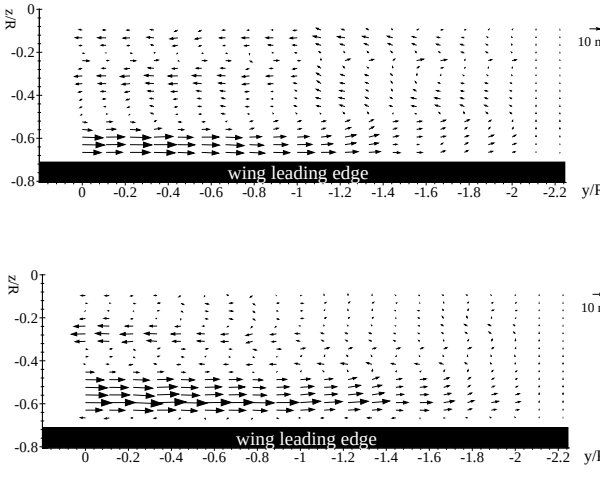

Figure 24: Spanwise flow at 9° azimuth for x/R= (a) 0.47 and (b) 0.72

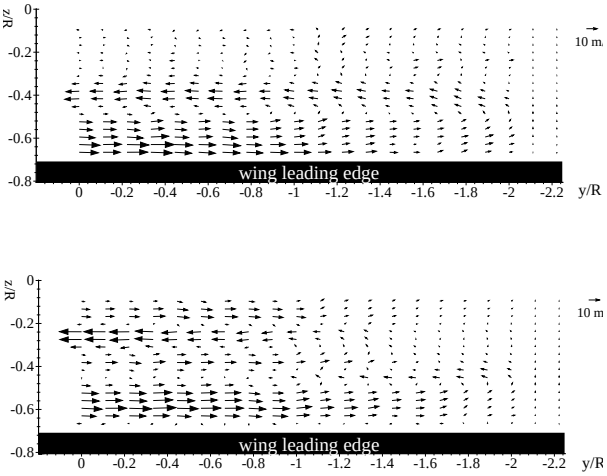

Figure 25: Spanwise flow at 324° azimuth for x/R= (a) 0.47 and (b) 0.72

Measurement Uncertainty

In full-scale measurements of this type, there are two objectives. The first is to get an overall view of the flow features and velocity field; the second is to get accurate measurements in specified regions. The techniques described here are adapted to these objectives. Over small areas, the measurement accuracy is limited by the pixel resolution of the camera: the present results were obtained using only a 512x512 pixel division of the image. The temporal resolution is limited by the need to get a vector with significant length in pixels, again limited by CCD and digitizer resolution. The primary source of error in the above measurements is the correction to be applied for misalignment between the two cameras. With all these errors included, velocity field accuracy is within 10%. On the other hand, the accuracy in vortex trajectories obtained with the same instrumentation is within the symbol sizes used in the plots.

Conclusions

Flow visualization in the wake of an isolated 2-bladed rotor showed vortex pairing and merging. The pairing process was found to be considerably delayed with increasing blade collective pitch as well as axial freestream velocity.

The isolated rotor test proved that when facility interference is eliminated, full-scale rotorcraft flowfields are extremely periodic even under near-hover conditions.

Application of SCV to rotorcraft flows in large facilities, under realistic Reynolds numbers and Mach numbers was demonstrated. SCV measurements in a radial plane showed inflow velocities of 12 m/s and wake velocities up to 15 m/s.

Promising results were obtained for the time averaged inflow and wake velocity profiles, using data obtained over a 2 m x 1.5 m area with light beam paths greater than 10 m, and camera to measurement plane distance of 5 m.

The planar SCV technique has been successfully used to generate phase-resolved, ensemble-averaged velocity fields in a 3D periodic rotor wake over a fixed wing.

Vorticity contours computed from the planar velocity data show the expected flow features. The divergence of the vortex trajectories, and their flowfield effects, are captured.

Results from the third component solver show the development of a spanwise wall jet above the wing due to wake interaction. This spanwise flow towards the RBS close to the wing surface turns upward and flows back towards the ABS approximately midway between the wing surface and rotor plane.

With these results, the measurement of velocity fields in the size and velocity range of full-scale rotorcraft flows, is demonstrated.

Acknowledgments

The authors wish to acknowledge Dr. Caradonna at NASA, Ames Research Center, Aeroflightdynamics Directorate who made the isolated rotor tests possible. This work was performed under Task 7.2 of the NRTC Rotorcraft Center of Excellence at Georgia Tech. The technical monitors are Dr. Yung Yu and Dr. Thomas Doligalski.

References

1. Caradonna, F., Henley, E., Silva, M., and Huang, S. with Komerath, N.M., Mahalingam, R., Reddy, U., Funk, R., Wong, O., Ames, R., Darden, L., Villareal, L. and Gregory, J., "Performance measurement and wake characteristics of a model rotor in axial flight", Journal of the American Helicopter Society, Vol. 44, no. 2, April 1999
2. Komerath, N.M., and Fawcett, P.A., "Planar velocimetry by spatial cross correlation: Theoretical basis and validation", AIAA 90-1634, 21st Fluid Dynamics, Plasma Dynamics and Lasers conference, Seattle, WA, June 1990.
3. Fawcett, P., Komerath, N.M., "Spatial Correlation Velocimetry in unsteady flows", AIAA 91-0271, 29th Aerospace Sciences Meeting, Reno, NV, Jan. 1991.
4. Fawcett, P.A., Funk, R.B. and Komerath, N.M., "Quantification of canard and wing interactions using Spatial Correlation Velocimetry", AIAA 92-2687, 10th Applied Aerodynamics Conference, Palo Alto, CA, June 1992.
5. Funk, R.B., Fawcett, P.A. and Komerath, N.M., "SCV Measurements in the wake of a rotor in hover and forward Flight", AIAA paper 93-3080, 24th Fluid Dynamics Conference, Orlando, FL, July 1993.
6. Griffin, M.H., Funk, R.B. and Komerath, N.M., "Turbulence measurements over large areas using Spatial Correlation Velocimetry", Proceedings of the Silver Symposium of the Flight Test Engineers Society, Patuxent River, MD, V-4-12, Aug. 1994.
7. Reddy, U.C., Matos, C.A., Mahalingam, R. and Komerath, N.M., "Whole-field velocity measurement in unsteady periodic flows", AIAA 97-2325, 15th AIAA Applied Aerodynamics Conference, Atlanta, GA, June 1997.
8. Funk, R.B., Crawford, U.C., Reddy, U.C. and Komerath, N.M., "Vortex induced transient separation on a lifting surface", AIAA94-0738, 32nd Aerospace Sciences Meeting and Exhibit, Reno, NV, Jan. 1994.
9. Funk, R.B., "Transient interaction between a rotor wake and a lifting surface", Ph.D. Thesis, School of Aerospace Engineering, Georgia Institute of Technology, 1995.